Nuclear Instruments and Methods in Physics Research A 1094 (2027) 172116

Contents lists available at ScienceDirect

Nuclear Inst. and Methods in Physics Research, A

journal homepage: www.elsevier.com/locate/nima

Full length article

Demonstrating the neutron radiation tolerance of the HV-MAPS TelePix2

Lucas Dittmann [a,*], Heiko Augustin [a], Sebastian Bachmann [a], Sebastian Dittmeier [a], Lennart Huth [b], David M. Immig [a], Ruben Kolb [a], Benedict Maisano [a,1], Ivan Perić [c], André Schöning [a], Niclas Sommerfeld [d], Marcel Stanitzki [b], Ulrich Uwer [a], Benjamin Weinläder [a], Arianna Wintle [b]

[a] Physikalisches Institut der Universität Heidelberg, INF 226, 69120 Heidelberg, Germany
[b] Deutsches Elektronen-Synchrotron DESY, Notkestraße 85, 22607 Hamburg, Germany
[c] Institut für Prozessdatenverarbeitung und Elektronik, KIT, Hermann-von-Helmholtz Platz 1, 76344 Eggenstein-Leopoldshafen, Germany
[d] Helmholtz-Institut für Strahlen- und Kernphysik Universität Bonn, Nussallee 14-16, 53115 Bonn, Germany

ARTICLE INFO

Keywords:
Pixel sensor
Monolithic
Radiation damage
NIEL
HV-CMOS

ABSTRACT

Future particle physics experiments such as experiments at the HL-LHC require radiation tolerant silicon pixel sensors. Currently, several monolithic pixel sensor technologies are under study as they enable tracking detectors with low material budget. One of such technologies are HV-MAPS, which are produced in 180 nm HV-CMOS processes.

The HV-MAPS TelePix2 has been irradiated with neutrons up to a fluence of $1 \times 10^{15}\,\mathrm{n_{eq}\,cm^{-2}}$ to evaluate the effect of radiation damage on this technology. The irradiated TelePix2 are evaluated in the lab in terms of leakage current and electronics response. Further, a measurement campaign was conducted at the DESY II test beam facility to determine the hit detection efficiency and the time resolution. After receiving a NIEL damage of $1 \times 10^{15}\,\mathrm{n_{eq}\,cm^{-2}}$, TelePix2 achieves a system time resolution of $\sigma_t \approx 2.4$ ns at a hit detection efficiency of $\epsilon_{\mathrm{hit}} > 99\%$, while keeping the noise rate below $10\,\mathrm{kHz\,cm^{-2}}$. The observed radiation damage follows the current understanding of NIEL damage on p-substrates.

1. Introduction

Tracking detectors for a high-rate environment require very light and radiation tolerant sensors with $\mathcal{O}$(ns) time resolution and $\mathcal{O}(10\,\mu\mathrm{m})$ spatial resolution, while keeping the noise rate and power consumption acceptable. High-Voltage Monolithic Active Pixel Sensors (HV-MAPS) [1] are a technology which can satisfy these requirements. These pixel sensors are implemented in a commercial HV-CMOS process allowing to apply a reverse bias voltage of $\mathcal{O}(100\,\mathrm{V})$ to the sensor diodes.

A use case of HV-MAPS is the proposed LHCb Upgrade II, where these sensors are the baseline design choice for the inner part of the main tracking system called Mighty Tracker [2]. The key performance parameter of these pixel sensors is a 99% hit detection efficiency within the 25 ns bunch crossing window of the LHC. This performance has to be achieved at an end of life non-ionising radiation damage corresponding to a neutron equivalent fluence of $3\times10^{14}\,\mathrm{n_{eq}\,cm^{-2}}$ while keeping the noise rate below $400\,\mathrm{kHz\,cm^{-2}}$ [3].

The TelePix2 sensor [4] discussed in the following is an HV-MAPS used at the DESY II test beam facility [5], serving as a timing and region-of-interest trigger plane for beam telescopes. Its design combines the most recent advancements of the HV-MAPS technology, demonstrating a timing resolution of $\sigma_t \approx 3.75$ ns [6], that has been optimised further. This positions TelePix2 as a promising candidate to study the radiation tolerance of this technology in context of an HV-CMOS sensors for LHCb.

2. Overview of TelePix2

TelePix2 is a monolithic pixel sensor implemented in the 180 nm HV-CMOS process of TSI Semiconductors. This section provides a brief overview of its features. A more detailed description can be found in [4]. The chip consists of 120 × 400 pixels with a pitch of 165 µm × 25 µm resulting in an active area of approximately 2 cm × 1 cm. The resistivity of the p-type substrate is chosen to be between 200 Ω cm and 400 Ω cm to allow for a depletion zone of 50–70 µm at a reverse bias voltage of $V_{\mathrm{bias}} = 130$ V before irradiation. The chips under test have been thinned down to a substrate thickness of 100 µm and 200 µm,

* Corresponding author.
E-mail address: dittmann@physi.uni-heidelberg.de (L. Dittmann).
[1] Now at Physikalisches Institut Universität Freiburg, Freiburg, Germany.

https://doi.org/10.1016/j.nima.2026.172116
Received 12 May 2026; Received in revised form 5 August 2026; Accepted 22 September 2026
Available online 10 October 2026
0168-9002/© 2026 The Authors. Published by Elsevier B.V. This is an open access article under the CC BY license (http://creativecommons.org/licenses/by/4.0/).
Open access funding enabled and organized by Projekt DEAL.

Table 1
Overview of the irradiated TelePix2 and their irradiation facility.

Fluence [$n_{eq}\,cm^{-2}$]	Sensor thickness [µm]	Facility
1×10^{13}	100	JSI
1×10^{14}	100	JSI
1×10^{14}	200	JGU
5×10^{14}[a]	100	JSI
5×10^{14}	200	JGU
1×10^{15}	100	JSI

[a] Due to broken bonds on the digital interface, the 100 µm thick TelePix2 irradiated at $5\times10^{14}\,n_{eq}\,cm^{-2}$ could only be used for leakage current measurements (Section 4.1).

leaving non-depleted material. Every pixel contains a charge sensitive amplifier and a comparator. The detection threshold of the comparator is set globally and can be fine-tuned per pixel. However, in this paper, no trimming of the pixel threshold is applied, as for sufficiently large depletion, no significant benefit is observed. Each pixel has a dedicated hit buffer in the periphery of the chip, which digitises the discriminated signals using a 4 ns time binning. The hit buffers are read by a hit driven readout operating at 1.25 Gbit/s.

3. Irradiation

To study the tolerance of the HV-MAPS technology to non-ionising energy loss (NIEL) TelePix2 have been irradiated with neutrons at the TRIGA MARK II reactor facilities of Jožef Stefan Institute (JSI), [7] Ljubljana and Johannes Gutenberg University (JGU), Mainz [8]. The 1 MeV equivalent neutron fluences range between $1\times10^{13}\,n_{eq}\,cm^{-2}$ and $1\times10^{15}\,n_{eq}\,cm^{-2}$ as listed in Table 1. A relative uncertainty on the neutron fluence of 10% is assumed. The irradiated chips have been annealed at 60 °C for 120 min prior to measurements presented here. Since the sensors were not powered during irradiation and thus no electrical fields were present in the transistor structures, significant TID damage from the photons present in the reactor is not expected to be observed after irradiation [9].

3.1. NIEL damage on p-type silicon

According to the review of NIEL damages in silicon [10], three main effects are expected for the operation of TelePix2 after irradiation.

Firstly, an increase of the leakage current in the sensor diode is expected, caused by additional levels in the energy band structure. This leakage current will increase the noise level of the detector, which can be mitigated by cooling.

Secondly, these additional energy levels can trap charges created by an ionising particle in the pixel diode, which will lead to less collected charge. Thus, a reduced hit detection efficiency is expected after irradiation.

Lastly, the NIEL damage will affect the effective resistivity of the silicon substrate. At low fluences, radiation induced acceptor removal will lead to an increase in substrate resistivity. At higher fluences other effects like the creation of deep acceptor-like defects become dominant and lead to a decrease of resistivity. As TelePix2 is mostly operated underdepleted, the increased resistivity at low fluences allows for larger depletion depth, whereas the decrease at higher fluences results in less depletion. The exact change in resistivity with NIEL damage cannot be predicted, as it depends on the initial substrate resistivity. However, measurements of p-type diodes [11] and similar HV-CMOS sensors [12] indicate that the resistivity could peak around a fluence of $1\times10^{14}\,n_{eq}\,cm^{-2}$.

In summary, a combination of counteracting effects on the sensor performance is expected. The radiation-induced change of the effective resistivity improves the performance for low fluences and degrades it for higher fluences. Charge trapping on the other side causes progressive deterioration.

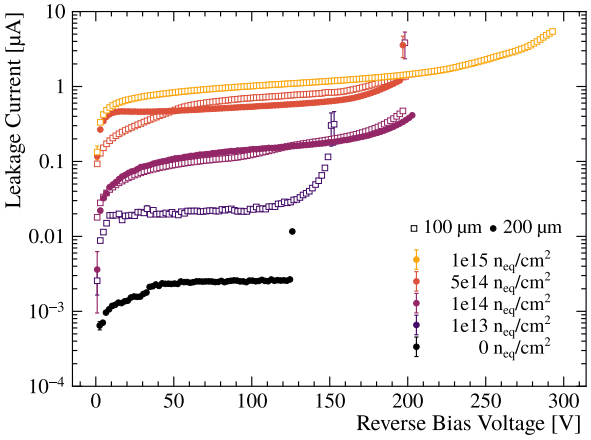


Fig. 1. IV characteristics of irradiated TelePix2 sensors at a temperature of −42 °C for a sensor thickness of 100 µm (unfilled) and 200 µm (filled). The measurement is stopped at a current limit of 10 µA.

4. Results

The TelePix2 chips are evaluated using the Heidelberg HV-MAPS data acquisition system [13–15]. The chips under test are operated at a supply voltage of 1.95 V and DAC settings which are optimised for time resolution[2]. All threshold values in the following sections are implicitly given in DAC units.

4.1. IV characteristics

Leakage current measurements as function of the reverse bias voltage (IV) were performed to study the impact of the neutron irradiation. For the IV-measurements the samples were cooled to −42 ± 4 °C. The uncertainty on the current measurement is the statistical uncertainty from 10 repeated measurements of the current. The IV-characteristic was recorded up to the current limit of 10 µA, which typically coincides with a breakdown behaviour. Fig. 1 presents the IV-characteristics of the irradiated TelePix2 alongside a non-irradiated reference sample. Note that the leakage current of the non-irradiated reference sample ($I_{leak} = \mathcal{O}(1\,nA)$) is on the order of the accuracy of the current measurement setup. The expected increase in leakage current due to defects in the silicon substrate created by neutron irradiation is observed.

The non-irradiated TelePix2 shows a breakdown behaviour at approximately 125 V at −42 °C. The breakdown voltage is determined using the k-factor method presented in [16]; a threshold value $k = 5$ is chosen here. A decrease of the breakdown voltage with decreasing temperature is observed, as the breakdown occurs at 145 V at room temperature. The observed temperature dependence is consistent with that of an avalanche breakdown. The breakdown voltage determined from the IV-characteristics is presented in Fig. 2. It is observed that the breakdown voltage shifts with irradiation fluence. The breakdown voltage increases significantly up to an irradiation fluence of $1\times10^{14}\,n_{eq}\,cm^{-2}$. Between $1\times10^{14}\,n_{eq}\,cm^{-2}$ and $5\times10^{14}\,n_{eq}\,cm^{-2}$ the breakdown voltage stays rather constant around $V_{bias} \approx 190$ V, while it increase up to about 275 V at a fluence of $1\times10^{15}\,n_{eq}\,cm^{-2}$. The shifting breakdown voltage is under investigation. It is likely caused by a change in the electric field due to changing effective resistivity, by a reduced impact ionisation due to charge trapping in defects, or by a combination of both effects. The increased breakdown voltage allows to operate the chips at higher reverse bias voltages after irradiation to compensate for changes in substrate resistivity.

[2] These settings have been optimised for higher reverse bias voltage than the results presented in [6].

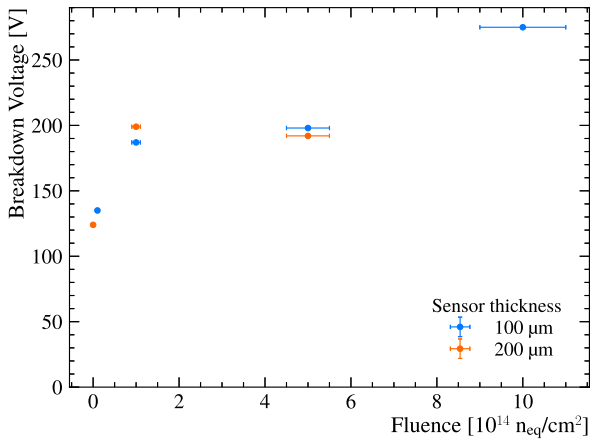


Fig. 2. Breakdown voltage of TelePix2 as a function of the irradiation fluence for a substrate thickness of 100 µm and 200 µm at $T = -42\,°C$.

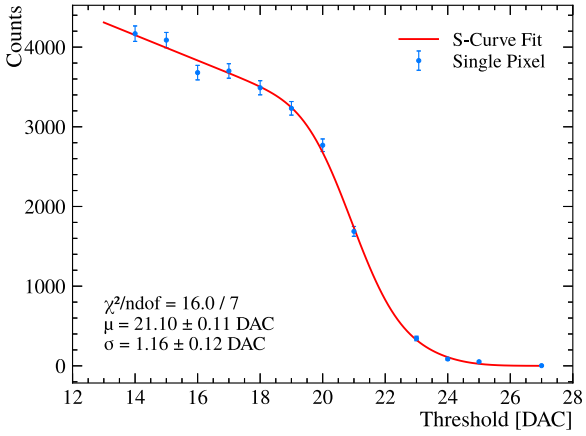


Fig. 3. Count rate of a single pixel of a TelePix2 irradiated at 5×10^{14} n_{eq} cm^{-2} exposed to a ^{55}Fe source as a function of the threshold fitted with the advanced S-curve model [17].

4.2. ^{55}Fe response

To assess whether neutron irradiation affects the working point of the pixel electronics, a calibration measurement is performed. For that, S-curve measurements with X-rays from an ^{55}Fe source are performed to determine the effective detection threshold of the irradiated TelePix2, which are then compared to a non-irradiated reference.

^{55}Fe emits two γ-lines, which can be used to gauge the effective threshold: the K_α line of approximately 5.9 keV and the K_β line of approximately 6.5 keV [18]. The energy deposition correspond to a charge generation of approximately 1.6 ke and 1.8 ke, respectively, in silicon. The K_α line is used to gauge the effective threshold, since its transition probability is about 7 times higher than that of the K_β line.

The S-curve is obtained by scanning the detection threshold while measuring the count rate of TelePix2 irradiated by a 500 MBq ^{55}Fe source, with an integration time of 120 s per threshold step. During the measurement, the TelePix2 are cooled to $-30 \pm 4\,°C$ to reduce the noise caused by leakage current in particular in case of the higher irradiated sensors. A reverse bias of 130 V is applied to allow for sufficient depletion of all samples. For every pixel, the count rate as a function of detection threshold is fitted with a phenomenological S-curve model, which takes charge sharing between pixels and the non-monochromaticity of ^{55}Fe into account. The S-curve model and fitting procedure is described in more detail in [17] based on [19]. The effective threshold μ described by the 50% value of the transition

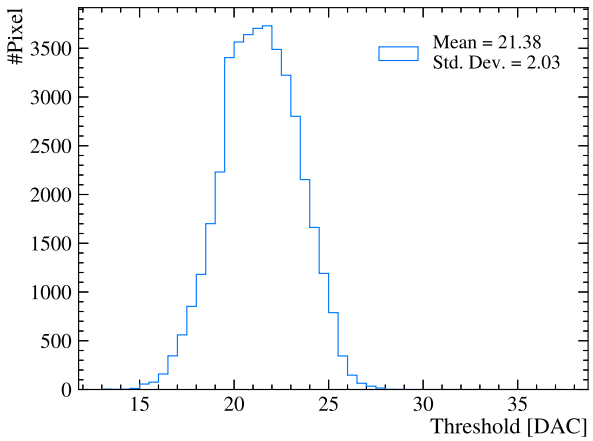


Fig. 4. Distribution of the effective threshold corresponding to 1.6 ke across the TelePix2 irradiated at 5×10^{14} n_{eq} cm^{-2}.

corresponds to the charge produced by the K_α x-ray of about 1.6 ke. The width of the transition is described by the parameter σ, which is a measure of the noise.

Fig. 3 shows the exemplary S-curve fit of one pixel. For thresholds below 17, a linear increase in count rate due to charge sharing can be observed. The detection threshold of 1.6 ke corresponds to a threshold of 21.

S-curves are measured and fitted for every pixel individually. Fig. 4 shows the thresholds corresponding to a charge of 1.6 ke for all pixels of one chip. The mean of all pixels is at 21.4 DAC values and the width of the distribution corresponds to 2 DAC values. Fig. 5 presents how the mean threshold varies as a function of the irradiation fluence, where the error bars in the y-direction indicate the standard deviation of the pixel distributions. The mean threshold differs between chips approximately by 1 DAC value, which is smaller than the pixel-to-pixel variation within a single chip, where the standard deviation is about 2 DAC values. This result indicates that the neutron irradiation does not affect the working point of the pixel electronics of TelePix2 significantly. As a single energy point is deemed insufficient, a calibration of the DAC scale to charge (e) is omitted here.

Similar to the mean detection threshold the noise parameter σ is extracted from the S-curve fits and the mean noise across the sensor is determined. Fig. 6 shows the mean noise as a function of the NIEL damage. The noise increases from 1.20 ± 0.21 DAC values before irradiation to a noise value of 1.83 ± 0.29 DAC values at a fluence of 1×10^{15} n_{eq} cm^{-2}, with the uncertainty given by the standard deviation across the chip. Under the assumption that the DAC-scale is linear for low values, the signal-to-noise ratio is calculated. The increasing noise leads to a decrease of the signal-to-noise ratio of the 1.6 ke signal from 17.5 before irradiation to 11.2 at a fluence 1×10^{15} n_{eq} cm^{-2}. The pixel capacitance is not expected to change with irradiation because at sufficiently high reverse bias voltages, the capacitance is dominated by the pixel geometry (cf. [20]). Thus, the observed increase in noise is qualitatively consistent with the expectations for increased leakage current due to NIEL damage.

4.3. Test beam

The irradiated sensors have also been evaluated at the DESY II test beam facility using a 4 GeV electron beam to assess their performance. A three layer MuPix11 [21] telescope and a scintillator have been used as reference system. The MuPix11 sensors offer a spatial resolution of $\sigma_x \approx 23$ µm and are used to reconstruct the electron tracks. These tracks are matched to the scintillator hits to obtain the time information of

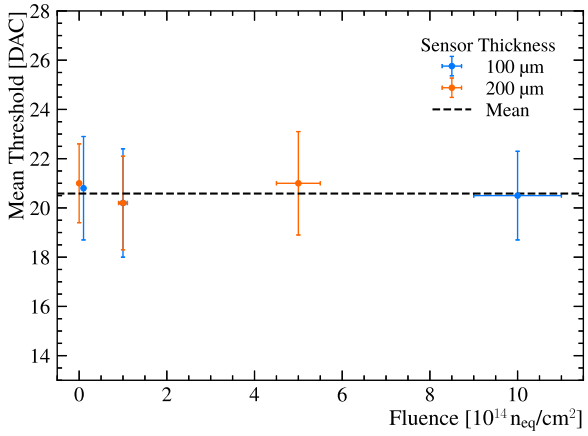


Fig. 5. Mean effective detection threshold corresponding to 1.6 ke as a function of irradiation fluence. The error bars in y-direction denote the standard deviation. The dashed line depicts the mean effective threshold across all sensors.

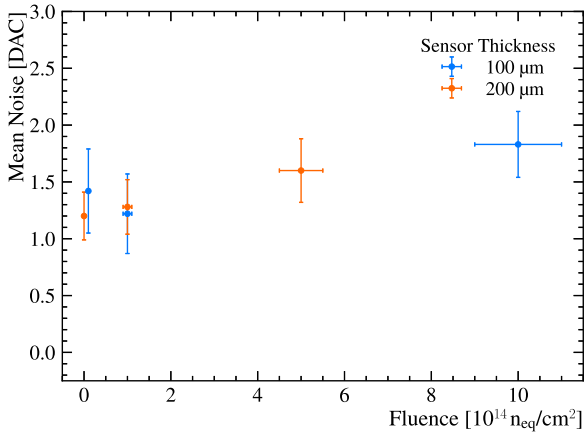


Fig. 6. Mean noise as a function of irradiation fluence. The error bars in y-direction denote the standard deviation.

the reconstructed tracks. The scintillator signal is sampled by the data acquisition system with 2 ns binning and has a time resolution $\sigma_t < 1$ ns.

The TelePix2 sensors under test have been cooled by fans in a dry ice ambient reaching temperatures between −10 °C and −45 °C. The temperature is measured on the chip carrier PCB using PT1000. The temperature offset between a running chip and the PT1000 is estimated by measurements with a thermal camera to be about 5–10 °C. Table 2 summarises the measured temperature by the PT1000 for the different measurement runs. The cooling setup based on dry ice does not allow a precise control of the temperature. To maximise the usage of beam time, any stable temperature was accepted as operation temperature. For the higher irradiated samples, lower temperature were required at high bias voltages to reduce the noise originating from leakage current.

The irradiated TelePix2 sensors are evaluated in terms of cluster size, hit detection efficiency and time resolution. The spatial resolution cannot be evaluated as the track resolution of the reference beam telescope is insufficient.

The recorded data is analysed using the corryvreckan framework [22]. A clustering algorithm is applied to group the hits on TelePix2 into hit clusters. The electron tracks reconstructed by the MuPix11 telescope are matched to clusters on the TelePix2 requiring a circular spatial distance of less than 700 µm and a time window around the measured scintillator time of less than 500 ns to achieve reasonable rejection for accidental matching. Pixels within 165 µm from the chip edge have been excluded from the analysis to suppress the impact of the limited tracking precision at the sensor edge.

Pixels with a noise rate exceeding 100 Hz/pixel have been masked during data taking. They correspond to less than 0.5% of active area of the respective sensors. The masked pixels however have not been excluded from the hit detection efficiency analysis.

Table 2
List of TelePix2 evaluated in test beam and operation temperature measured on the chip carrier PCB for the nominal reverse bias voltage of 130 V and at maximum reverse bias.

Fluence	Thickness	Temperature [°C]	
[n_{eq} cm^{-2}]	[µm]	Nominal bias	Maximum bias
0	200	−25	–
1×10^{13}	100	−25	−10
1×10^{14}	100	−35	−20
1×10^{14}	200	−30	−30
5×10^{14}	200	−30	−40
1×10^{15}	100	−35	−45

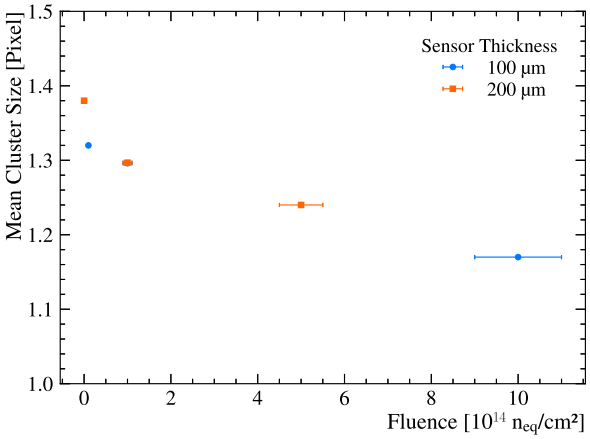


Fig. 7. The mean cluster size of clusters associated to a particle track as a function of the neutron fluence at V_{bias} = 130 V and Thr = 17. The points of the 100 µm and 200 µm thick TelePix2 irradiated at 1×10^{14} n_{eq} cm^{-2} are overlapping.

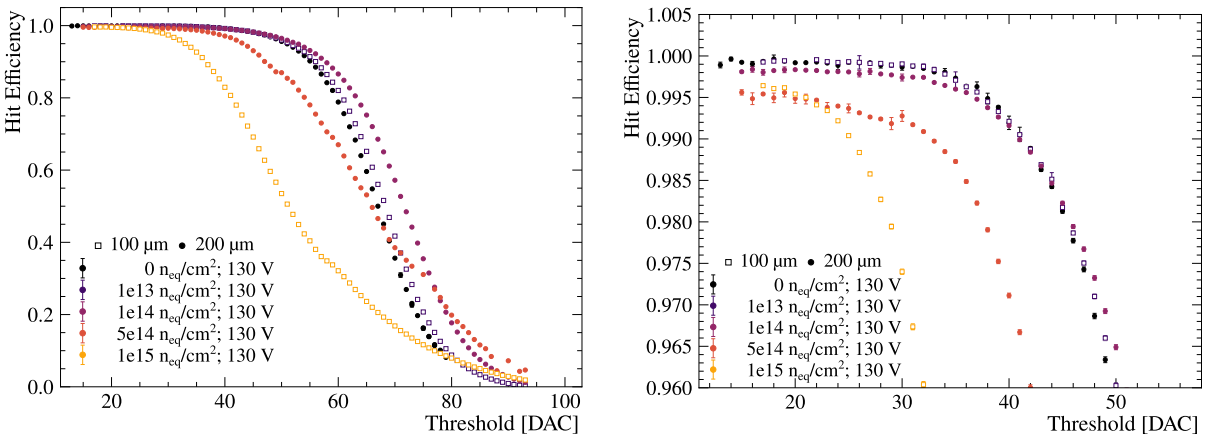
4.3.1. *Cluster size*

The size of clusters on TelePix2 associated to electron tracks is studied as a function of the irradiation fluence. Due to the position of the sensors under test within the telescope these tracks pass the sensors essentially perpendicular. Changes in the cluster size can indicate whether radiation damages affect the charge collection.

The mean cluster size for all sensors is compared at a reverse bias voltage V_{bias} = 130 V and a detection threshold Thr = 17, at which all chips are fully efficient ($\epsilon_{hit} > 99\%$). Fig. 7 shows the mean cluster size as a function of the neutron fluence. The non-irradiated TelePix2 has a mean cluster size of 1.36. The mean cluster size decrease asymptotically with the NIEL-induced damage to a mean cluster size of 1.17 at 1×10^{15} n_{eq} cm^{-2}. This reduced charge sharing can be attributed to the trapping of charges in radiation induced defects.

Also, the ratio between depleted and non-depleted material affects the observed cluster size, as diffusion in the non-depleted material contributes to the signal in non-irradiated HV-MAPS [17]. The change of effective resistivity by NIEL (see Section 3.1) results in samples operated at the same reverse bias voltage but irradiated at different fluences having different depletion depth.

From Fig. 7 it is seen that there is no significant difference in cluster size between the 100 µm and the 200 µm up to a neutron fluence of 1×10^{14} n_{eq} cm^{-2} irradiated TelePix2. We therefore conclude that the difference in size of the non-depleted zone is not the principal factor driving the cluster size.



(a) Hit efficiency as a function of the detection threshold.

(b) Zoom-in of the hit efficiency as a function of the detection threshold.

Fig. 8. Hit detection efficiency as function of the threshold for different neutron irradiation fluences at a bias voltage of 130 V. Unfilled squares mark sensors with a thickness of 100 µm, while circles indicate 200 µm thick sensors.

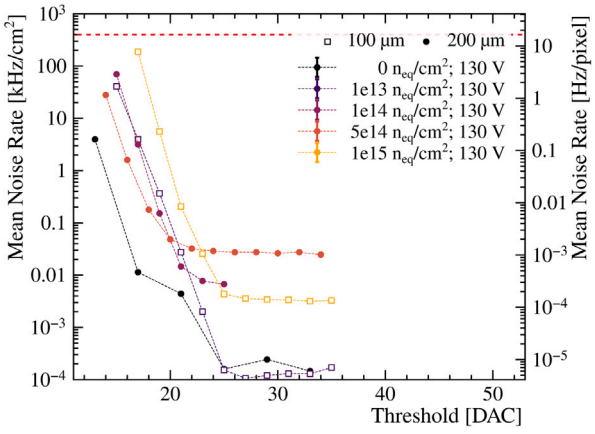


Fig. 9. Mean noise rate as a function of the detection threshold at a bias voltage of 130 V. Unfilled squares mark sensors with a thickness of 100 µm, while circles indicate 200 µm thick sensors. The dashed red line indicates the noise limit of the LHCb Mighty Tracker.

4.3.2. Hit detection efficiency

The hit detection efficiency of TelePix2 has been studied as a function of the threshold for the different neutron fluences. The hit detection efficiency is defined as the fraction of particle tracks reconstructed by the reference telescope that can be associated with a hit cluster on TelePix2, relative to all reconstructed tracks passing through the active sensor area.

The hit detection efficiency as a function of the detection threshold at the nominal reverse bias voltage of 130 V is shown in Fig. 8(a). The deviation from full efficiency is consistent with the expectation from the fraction of masked pixels, which is between 0.01% and 0.47%.

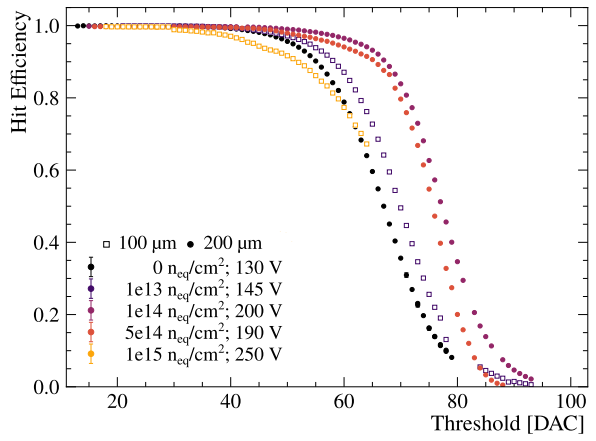
The corresponding mean noise rate to these thresholds is shown in Fig. 9. The noise count rate is measured over a time interval of 62 s with the electron beam turned off. The noise is only measured for lower thresholds where a significant noise rate is observed. Due to the increasing noise rate with irradiation the lowest operational threshold shifts to higher values with neutron fluence. At a threshold which corresponds to a mean noise rate of <0.01 Hz/Pixel (<0.1 kHz cm^{-2}) all irradiated samples achieve a hit detection efficiency of $\epsilon_{\text{hit}} > 99\%$.

Furthermore, the length of the efficiency plateaus vary with irradiation fluence (see Fig. 8). From the measurements in Section 4.2, it can be excluded that this difference in hit detection efficiency is caused by a change of the effective detection threshold. Thus, this effect probably arises from a difference in signal amplitude. As explained in Section 3.1, the depletion depth of TelePix2 is affected by NIEL-induced changes in the effective substrate resistivity. Consequently, the depletion volume changes, resulting in a difference in the charge collected per incident particle. Further, this charge is also affected by trapping in radiation induced defects.

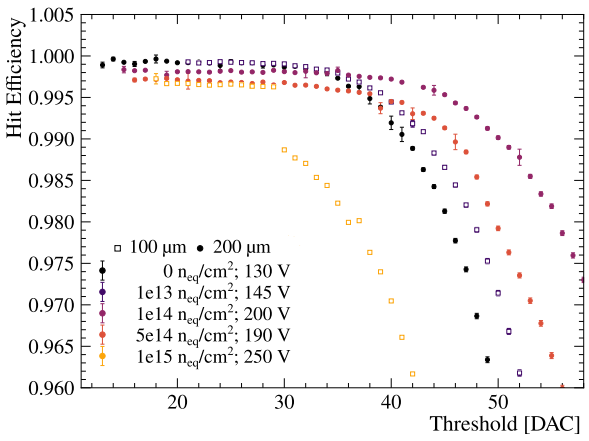
The TelePix2 sensors irradiated to 1×10^{13} n$_{\text{eq}}$ cm^{-2} and 1×10^{14} n$_{\text{eq}}$ cm^{-2} achieve 99% hit detection efficiency for threshold values higher than the non-irradiated reference sample, which corresponds to more collected charge. This is compatible with a larger depletion zone caused by a higher resistivity, arising from acceptor removal by neutron radiation. In contrast, the 5×10^{14} n$_{\text{eq}}$ cm^{-2} and 1×10^{15} n$_{\text{eq}}$ cm^{-2} irradiated samples lose efficiency for lower threshold values than the non-irradiated sample, which could correspond to less collected charge as result of a smaller depletion zone due to a decrease in effective resistivity and by charge trapping in defects.

As seen in Fig. 2, the breakdown voltage increases with the neutron fluence, allowing a higher reverse bias voltage for higher neutron fluences. A reverse bias voltage close to the breakdown voltage allows to recover the performance of the higher irradiated samples to a similar level as the non-irradiated chip. The hit detection efficiency as a function of the threshold for maximum reverse bias voltages is shown in Fig. 10(a). The higher bias voltage leads to an increase in the noise rate due to the higher leakage current, which is mitigated by cooling the samples which have seen a larger neutron fluence to colder temperatures (see Table 2). The corresponding noise rate for the different thresholds are shown in Fig. 11. An operation point with a mean noise rate of less than 0.5 Hz/Pixel (≈10 kHz cm^{-2}) and a hit detection efficiency of $\epsilon_{\text{hit}} > 99\%$ is possible for all samples.

Fig. 12 compares the hit detection efficiency of the 100 µm and 200 µm thick 1×10^{14} n$_{\text{eq}}$ cm^{-2} irradiated TelePix2. The performance of both chips is comparable at reverse bias voltage of 130 V. Increasing the bias voltage of the 100 µm thick chip to 180 V does not extend the efficiency plateau with $\epsilon_{\text{hit}} > 99\%$ significantly to higher threshold values. On the other side, by increasing the reverse bias voltage for the 200 µm thick TelePix2 the efficiency plateau can be extended to higher threshold values. This leads to the assumption that the 100 µm thick



(a) Hit efficiency as a function of the detection threshold.



(b) Zoom-in of the hit efficiency as a function of the detection threshold.

Fig. 10. Hit detection efficiency as function of the threshold for different neutron irradiation fluences at the maximum possible bias voltage. Unfilled squares mark sensors with a thickness of 100 µm, while circles indicate 200 µm thick sensors.

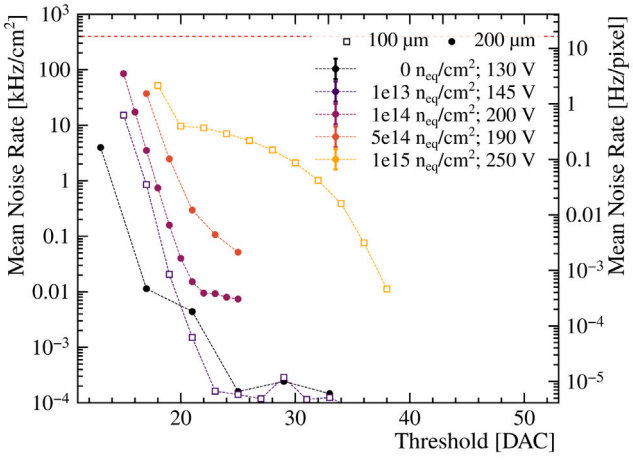


Fig. 11. Mean noise rate as a function of the detection threshold at the maximum possible bias voltage. Unfilled squares mark sensors with a thickness of 100 µm, while circles indicate 200 µm thick sensors. The dashed red line indicates the noise limit of the LHCb Mighty Tracker.

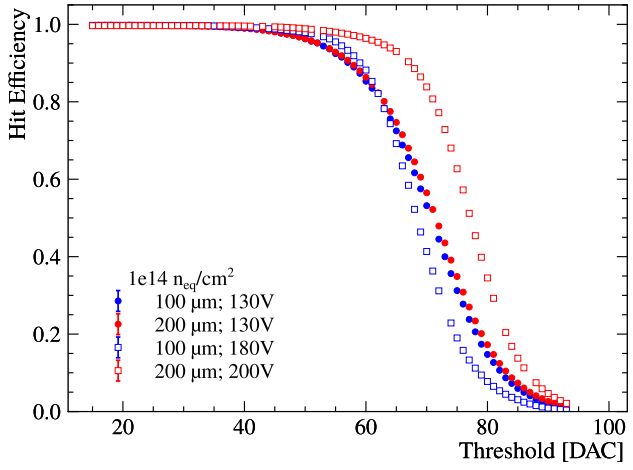


Fig. 12. Hit detection efficiency as function of the threshold of a 100 µm and 200 µm thick TelePix2 irradiated to 1×10^{14} n_{eq} cm^{-2} for a reverse bias of 130 V and for maximum bias.

sensor is nearly fully depleted at a bias voltage of 130 V and irradiation fluence of 1×10^{14} n_{eq} cm^{-2}.[3]

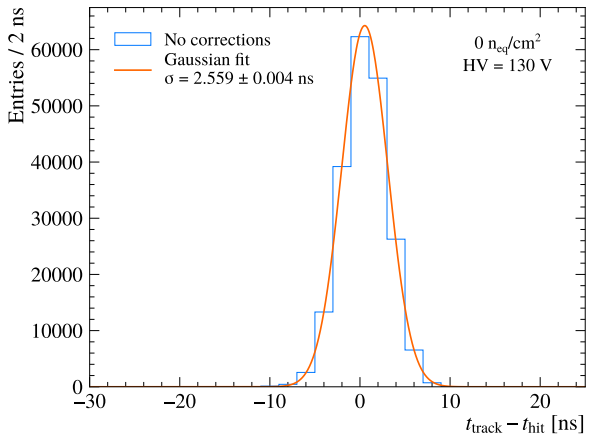
4.3.3. Time resolution

The time resolution is determined by a Gaussian fit to the difference between the scintillator based timestamp of the matched tracks and the hit timestamp of TelePix2. The absolute delay between track t_{track} and hit time t_{hit} is dominated by DAQ effects. The measured time resolution includes the resolution of the reference system of about 1 ns, which is not corrected for. Corrections of timewalk and of the pixel position do not improve the time resolution of TelePix2 significantly at low thresholds, thus no corrections are applied in this paper.

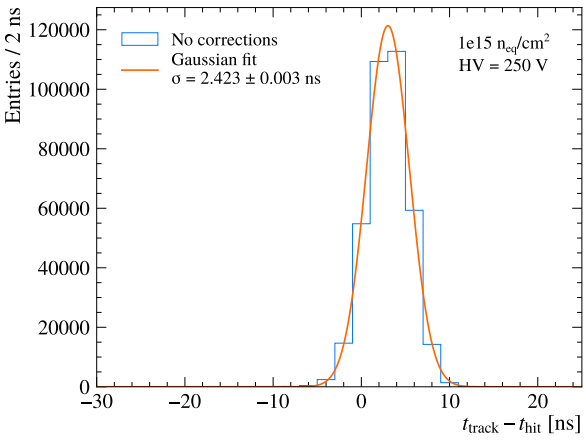
As seen in Fig. 13, the Gaussian fit describes the data well. For high thresholds (Thr > 33) the distribution is distorted by a tail created from timewalk. The Gaussian fit yields a time resolution of $\sigma_t = (2.559 \pm 0.004)$ ns at a reverse bias voltage of $V_{bias} = 130$ V and a threshold of Thr = 13 for the non-irradiated TelePix2 with a thickness of 200 µm (Fig. 13(a)). The uncertainty is given by the statistical uncertainty of the fit. Fig. 13(b) depicts the time resolution of the 1×10^{15} n_{eq} cm^{-2} irradiated TelePix2 with a thickness of 100 µm at a bias voltage of 250 V and a threshold of Thr = 17. Also in this case, the data is well described by a Gaussian fit. The fit yields a time resolution of $\sigma_t = (2.423 \pm 0.003)$ ns, where the uncertainty stems from the statistical uncertainty of the fit.

Fig. 14 shows the time resolution of the irradiated TelePix2 measured as a function of the detection threshold for a reverse bias of $V_{bias} = 130$ V (Fig. 14(a)) and for the maximum possible bias voltage (Fig. 14(b)). The measured time resolution deteriorates with increasing threshold due to timewalk. The time resolution changes with irradiation similarly to the hit detection efficiency. At the same threshold and reverse bias voltage the samples irradiated to 1×10^{13} n_{eq} cm^{-2} and 1×10^{14} n_{eq} cm^{-2} achieve a better time resolution than the non-irradiated reference, presumably caused by a larger signal due to a larger depletion zone. By increasing the reverse bias voltage to the maximum possible voltage, the time resolution of the irradiated TelePix2 sensors improves with respect to the non-irradiated sensor at a similar threshold. This is likely caused by the larger depletion zone created by the higher bias voltage. All samples achieve a time resolution of $\sigma_t < 2.7$ ns at lowest possible detection threshold. Note the jump in the

[3] In contrast to non-irradiated HV-MAPS, full depletion is not observed in the IV characteristic (Fig. 1) after irradiation due to the already high leakage current.

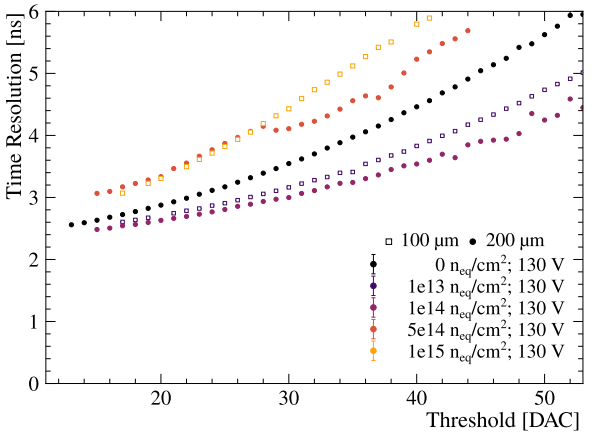


(a) Time difference of a non-irradiated TelePix2 with a thickness of 200 µm.

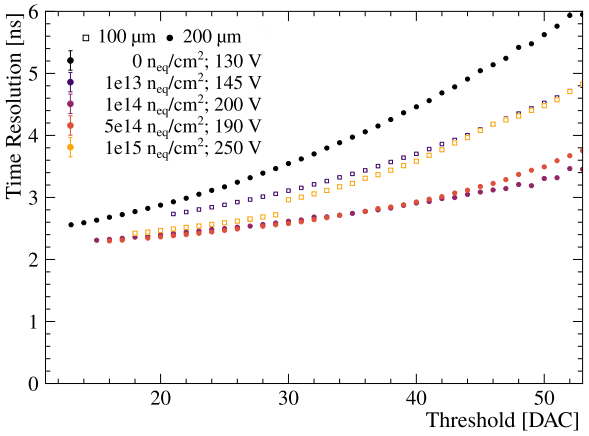


(b) Time difference of a 1×10^{15} n_{eq} cm^{-2} irradiated TelePix2 with a thickness of 100 µm.

Fig. 13. Difference between track time t_{track} and hit time t_{hit} fitted with a Gaussian for a non-irradiated and a 1×10^{15} n_{eq} cm^{-2} irradiated TelePix2.



(a) Time resolution at reverse bias of 130 V.



(b) Time resolution at maximum reverse bias.

Fig. 14. Time resolution as a function of the threshold for different fluences at nominal and highest possible reverse bias. The error bars denote the statistical uncertainty of the fit. Unfilled squares mark sensors with a thickness of 100 µm, while circles indicate 200 µm thick sensors.

measurement of the 1×10^{15} n_{eq} cm^{-2} (Fig. 14(b)), which was caused by loss in cooling which led to a temperature increase by 10 °C. The change in the resolution of the 5×10^{14} n_{eq} cm^{-2} reverse biased at 130 V (Fig. 14(a)) at a threshold of thr = 29 is not fully understood but assumed to originate from the scintillators used as time reference.

4.3.4. In-time efficiency

For the application of the HV-MAPS for LHCb Upgrade II, the ability to tag a particle to the correct 25 ns bunch crossing, which is further referred to as in-time efficiency ϵ_{25ns} in the following, is the figure of merit rather than time resolution and hit detection efficiency alone. The in-time efficiency is determined by the tracks matched to TelePix2 with a hit time in a ±12.5 ns window around the mean of the Gaussian distribution fitted in the previous section over the total number of tracks intersecting TelePix2. The 25 ns window is centred around the Gaussian mean to correct for the delay between the time reference and TelePix2. This approach underestimates the in-time efficiency for thresholds where timewalk is present. The uncertainty given on the in-time efficiency is purely statistical and does not include this systematic contribution.

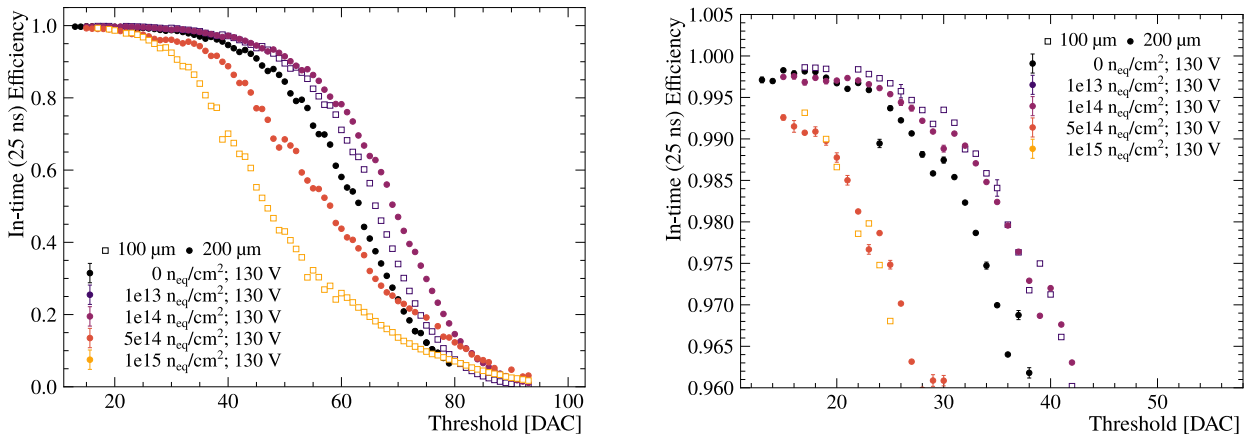
All samples reach an in-time efficiency of $\epsilon_{25ns} > 99\%$ for a reverse bias voltage of 130 V (Fig. 15) and for the maximum bias voltage (Fig. 16). Since the in-time efficiency combines hit detection efficiency and time resolution the same behaviour to the neutron irradiation as for those individual quantities can be observed.

With achieving an in-time efficiency of $\epsilon_{25ns} > 99\%$ and mean noise rate of less than 10 kHz cm^{-2} after an irradiation with a neutron fluence of 1×10^{15} n_{eq} cm^{-2} TelePix2 shows that the HV-MAPS technology fulfils the performance requirements of high rate experiments like LHCb Upgrade II.

5. Conclusion

The tolerance of TelePix2 to non-ionising radiation was tested up to a fluence of 1×10^{15} n_{eq} cm^{-2}. A hit detection efficiency $\epsilon_{hit} > 99\%$ and a system time resolution better than 2.4 ns have been observed, even without correction for the 1 ns reference time resolution.

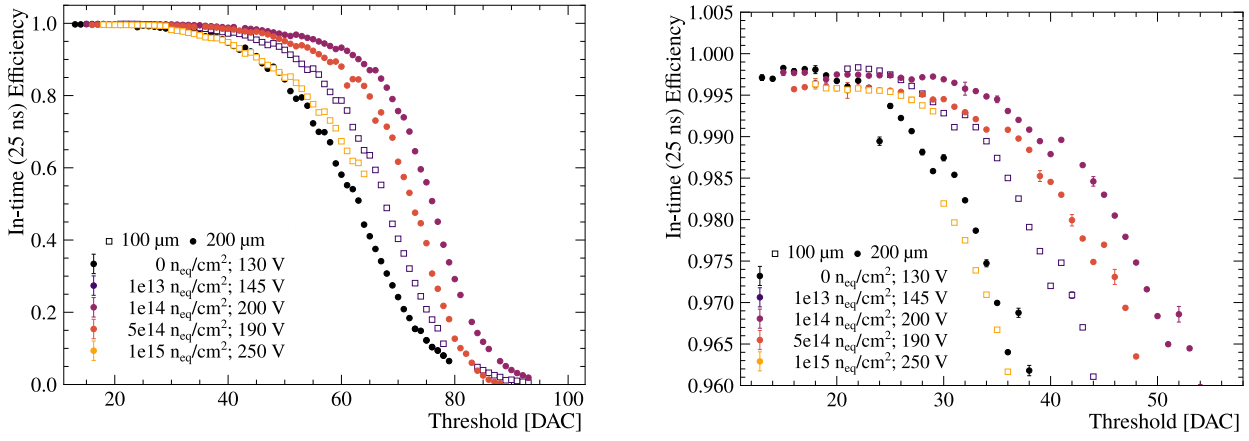
Furthermore, non-ionising radiation has no observable effect on the pixel electronics of TelePix2. There is evidence that the effective doping concentration changes with non-ionising radiation damage which leads to a performance boost around a neutron fluence of 1×10^{14} n_{eq} cm^{-2}. It is observed that the breakdown voltage of TelePix2 increases with non-ionising radiation damage. This allows to recover performance after



(a) In-time efficiency as a function of the threshold.

(b) Zoom-in of the in-time efficiency as a function of the threshold.

Fig. 15. In-time efficiency as a function of the threshold at nominal bias of 130 V for the different irradiation levels. Unfilled squares mark sensors with a thickness of 100 µm, while circles indicate 200 µm thick sensors.



(a) In-time efficiency as a function of the threshold.

(b) Zoom-in of the in-time efficiency as a function of the threshold.

Fig. 16. In-time efficiency as a function of the threshold at maximum bias for the different irradiation levels. Unfilled squares mark sensors with a thickness of 100 µm, while circles indicate 200 µm thick sensors.

irradiation by applying a higher reverse bias voltage. The observed effects of NIEL damage are in accordance with the current understanding of p-type substrates.

These results demonstrate that the HV-MAPS technology has the ability to be employed in an LHC environment, where an in-time efficiency of $\epsilon_{25\text{ns}} > 99\%$ is required.

CRediT authorship contribution statement

Lucas Dittmann: Writing – original draft, Visualization, Validation, Software, Resources, Investigation, Formal analysis, Data curation, Conceptualization. **Heiko Augustin:** Writing – review & editing, Supervision, Software, Resources, Methodology. **Sebastian Bachmann:** Writing – review & editing, Supervision, Project administration. **Sebastian Dittmeier:** Software. **Lennart Huth:** Writing – review & editing, Software, Resources, Methodology, Funding acquisition. **David M. Immig:** Writing – review & editing, Software, Formal analysis, Data curation. **Ruben Kolb:** Writing – review & editing, Software, Investigation. **Benedict Maisano:** Investigation. **Ivan Perić:** Resources, Funding acquisition, Conceptualization. **André Schöning:** Resources, Project administration. **Niclas Sommerfeld:** Writing – review & editing, Resources. **Marcel Stanitzki:** Writing – review & editing, Funding acquisition. **Ulrich Uwer:** Writing – review & editing, Supervision, Methodology, Funding acquisition, Conceptualization. **Benjamin Weinläder:** Resources. **Arianna Wintle:** Investigation.

Declaration of competing interest

The authors declare that they have no known competing financial interests or personal relationships that could have appeared to influence the work reported in this paper.

Acknowledgements

We acknowledge support by the Deutsche Forschungsgemeinschaft (DFG, German Research Foundation) under Germany's Excellence Strategy – EXC 2121 "Quantum Universe" – 390833306 and by the Bundesministerium für Forschung, Technologie und Raumfahrt (BMFTR, German Federal Ministry of Research, Technology and Space). The measurements leading to these results have been performed at the

Test Beam Facility at DESY Hamburg (Germany), a member of the Helmholtz Association (HGF). We acknowledge the support of the reactor facilities of JSI Ljubljana and JGU Mainz in irradiating the samples.

Data availability

Data will be made available on request.

References

[1] I. Perić, A novel monolithic pixelated particle detector implemented in high-voltage CMOS technology, NIM-A 582 (3) (2007) 876–885, http://dx.doi.org/10.1016/j.nima.2007.07.115, VERTEX 2006.

[2] LHCb Collabration, Framework TDR for the LHCb Upgrade II, Tech. Rep., CERN, Geneva, 2021, http://dx.doi.org/10.17181/CERN.NTVH.Q21W.

[3] LHCb collaboration, LHCb Upgrade II Scoping Document, Tech. Rep., CERN, Geneva, 2024, http://dx.doi.org/10.17181/CERN.2RXP.HDK0.

[4] L. Huth, et al., TelePix2: Full scale fast region of interest trigger and timing for the EUDET-style telescopes at the DESY II test beam facility, NIM-A 1080 (2025) 170720, http://dx.doi.org/10.1016/j.nima.2025.170720.

[5] R. Diener, et al., The DESY II test beam facility, NIM-A 922 (2019) 265–286, http://dx.doi.org/10.1016/j.nima.2018.11.133.

[6] H. Augustin, et al., Timing characterisation of TelePix2, J. Instrum. 20 (06) (2025) C06071, http://dx.doi.org/10.1088/1748-0221/20/06/C06071.

[7] L. Snoj, et al., A half-century of nuclear research, education and training: Story of the JSI TRIGA reactor, Ann. Nucl. Energy 214 (2025) 111122, http://dx.doi.org/10.1016/j.anucene.2024.111122.

[8] K. Eberhardt, C. Geppert, The research reactor TRIGA Mainz – a strong and versatile neutron source for science and education, Radiochim. Acta 107 (7) (2019) 535–546, http://dx.doi.org/10.1515/ract-2019-3127.

[9] J.R. Schwank, et al., Radiation effects in MOS oxides, IEEE Trans. Nucl. Sci. 55 (4) (2008) 1833–1853, http://dx.doi.org/10.1109/TNS.2008.2001040.

[10] M. Moll, Displacement damage in silicon detectors for high energy physics, IEEE Trans. Nucl. Sci. 65 (8) (2018) 1561–1582, http://dx.doi.org/10.1109/TNS.2018.2819506.

[11] M. Moll, Acceptor removal - Displacement damage effects involving the shallow acceptor doping of p-type silicon devices, PoS Vol. Vertex2019 (2020) 027, http://dx.doi.org/10.22323/1.373.0027.

[12] M. Franks, Design and characterisation of High-Voltage CMOS (HV-CMOS) detectors for particle physics experiments (Ph.D. thesis), University of Liverpool, 2022, http://dx.doi.org/10.17638/03165214.

[13] H. Augustin, et al., The MuPix telescope: A thin, High-Rate tracking telescope, J. Instrum. 12 (01) (2017) C01087, http://dx.doi.org/10.1088/1748-0221/12/01/C01087.

[14] S. Dittmeier, Fast Data Acquisition for Silicon Tracking Detectors at High Rates (Ph.D. thesis), Heidelberg University, Heidelberg, 2018, http://dx.doi.org/10.11588/heidok.00025791.

[15] L. Huth, A High Rate Testbeam Data Acquisition System and Characterization of High Voltage Monolithic Active Pixel Sensors (Ph.D. thesis), Heidelberg University, Heidelberg, 2018, http://dx.doi.org/10.11588/heidok.00025785.

[16] N. Bacchetta, et al., Improvement in breakdown characteristics with multiguard structures in microstrip silicon detectors for CMS, NIM-A 461 (1) (2001) 204–206, http://dx.doi.org/10.1016/S0168-9002(00)01207-9, 8th Pisa Meeting on Advanced Detectors.

[17] D.M. Immig, Straggling in Underdepleted Ultra-Thin Silicon HV-CMOS Sensors (Ph.D. thesis), Heidelberg University, Heidelberg, 2026, http://dx.doi.org/10.11588/heidok.00038033.

[18] A.J.M. Plompen, et al., The joint evaluated fission and fusion nuclear data library, JEFF-3.3, Eur. Phys. J. A 56 (7) (2020) 181, http://dx.doi.org/10.1140/epja/s10050-020-00141-9.

[19] E.J. Schioppa, The color of X-rays: Spectral X-ray computed tomography using energy sensitive pixel detectors (Ph.D. thesis), Box Press, Universiteit van Amsterdam, 2014.

[20] I. Perić, et al., High-voltage CMOS active pixel sensor, IEEE J. Solid-State Circuits 56 (8) (2021) 2488–2502, http://dx.doi.org/10.1109/JSSC.2021.3061760.

[21] T.T. Rudzki, et al., An ultra-light helium cooled pixel detector for the Mu3e experiment, J. Instrum. 18 (10) (2023) C10022, http://dx.doi.org/10.1088/1748-0221/18/10/C10022.

[22] D. Dannheim, et al., Corryvreckan: a modular 4D track reconstruction and analysis software for test beam data, J. Instrum. 16 (03) (2021) P03008, http://dx.doi.org/10.1088/1748-0221/16/03/P03008.